

Selenium Biogeochemical Cycling and Fluxes in the Hyporheic Zone of a Mining-Impacted Stream

LIBBIE L. ORAM,[†]
DANIEL G. STRAWN,^{*, †, ‡}
MATTHEW J. MORRA,^{†, §} AND
GREGORY MÖLLER[†]

Environmental Sciences Program, and Plant, Soil and Entomological Sciences Department, University of Idaho, Moscow, Idaho 83844-2339

Received January 15, 2010. Revised manuscript received April 10, 2010. Accepted April 23, 2010.

The influence of hyporheic exchange on selenium (Se) biogeochemistry and mobility in sediments is unknown. A multiscale investigation of Se biogeochemistry in the hyporheic zone of East Mill Creek (EMC), southeastern Idaho, USA, was performed using *in situ* surface water and pore water geochemical measurements, a field-based stream tracer test, and energy-dependent micro synchrotron X-ray fluorescence (μ -SXRF) measurements of Se speciation in sediments. The active hyporheic zone was determined to be 12 ± 3 cm. Pore water redox profiles indicated that a transition to suboxic conditions begins at approximately 6 cm. Modeling pore water Se and solid phase analysis suggested Se uptake is occurring. Micro-SXRF analysis of sediments showed reduced elemental Se or selenides throughout the profile and selenite in surface sediments. Field geochemical measurements and microscale analysis both support the hypothesis that reduction in the hyporheic zone promotes sequestration of surface water Se.

Introduction

Selenium contamination of aquatic ecosystems is a significant global concern, and aqueous Se is an important exposure pathway at multiple trophic levels (1). In the Blackfoot River watershed in southeastern Idaho, USA, sedimentary waste rock from phosphate mining contains elevated concentrations of Se. Weathering of the waste rock has resulted in widespread Se contamination of areas within the contiguous watershed (2), including in sediments (3), aquatic invertebrates, and fish from several streams (4). However, linkage between elevated Se and aquatic ecosystem toxicity is unclear because speciation and other site-specific biogeochemical and hydrological factors are unknown (1).

In the environment, Se exists in four different oxidation states (-II, 0, IV, and VI), each with varying reactivity, mobility, and bioavailability. Both inorganic and organic Se species are common, and speciation is ecosystem and microenvironment specific (1). Microorganisms, algae, insects, plants, and animals can bioaccumulate and change the species of Se through metabolism, thus, altering the availability and potential toxicity (1).

* Corresponding author phone: 208-885-2713; e-mail: dgstrawn@uidaho.edu.

[†] Environmental Sciences Program, University of Idaho.

[‡] Plant, Soil and Entomological Sciences Department, University of Idaho.

To assess the ability of streams to attenuate or release Se, it is critical to understand Se biogeochemical reactions occurring at the surface water–groundwater interface, the hyporheic zone. Mass flux between the groundwater and surface water, termed hyporheic exchange, facilitates the transport of contaminants across the sediment–water interface (5). However, concentrations of Se in the hyporheic zone may also be affected by sequestration and release reactions, including: biological alkylation, precipitation/dissolution, adsorption/desorption, and abiotic redox reactions (6, 7).

Field measurements allow *in situ* investigation of interactions between flow, transport, and biogeochemical processes (8). Stream-tracer experiments can be used to define the hydrologic exchange within hyporheic zones (8) and to assess the fate of contaminants in streams (9). To predict Se fluxes, it is necessary to know the species of sediment Se in addition to hydrologic exchange. Selenium speciation can be measured using energy-dependent micro synchrotron X-ray fluorescence mapping (μ -SXRF), which has low detection limits, requires no sample pretreatment, and minimizes radiation damage (3, 10, 11).

Studies have investigated Se geochemistry in sediments from lentic ecosystems (7, 12–14), and hyporheic exchange has been established as an important aspect of biogeochemical cycles of other elements (15–17). No studies have characterized Se biogeochemistry and flux in the hyporheic zone of lotic ecosystems. In the current study, a multiscale investigation of Se in the hyporheic zone of East Mill Creek (EMC) in the Blackfoot River watershed was performed using surface water and pore water geochemical measurements, a field-based tracer, and μ -SXRF measurements of Se speciation.

Materials and Methods

Site Description. In June 2008 and August 2008, a 20 m stretch of EMC in lower Mill Canyon was sampled at three sites located ~ 2.25 km from North Maybe Canyon mine at 1990 m elevation (Supporting Information available). Samples for sediment Se speciation were also collected in September 2007. Depositional zone sites, common in this stretch of EMC, were chosen to allow triplicate samplers to be inserted to 18 cm. At sampling sites, the stream was a low-gradient, meandering, riffle/pool stream, less than 0.5 m deep and 1 m wide. Groundwater flow paths are parallel to the creek (18).

Sampling. Unfiltered and filtered ($0.45\text{ }\mu\text{m}$) surface water (SW) samples were collected (Supporting Information available). Dissolved O₂, pH, and temperature were measured in the SW using calibrated probes. Temperature profiles were collected at each site by inserting a 1.2 m temperature probe into the sediment and taking readings every 5 cm. Stream velocity was measured using a Marsh-McBirney velocity meter, and stream discharge was determined using the velocity-area method.

Pore water (PW) samples were collected with triplicate Minipoint samplers (19) at each site. Three Minipoint apparatuses, each with six mini drivepoints set at 3 cm increments (Supporting Information available), were pushed into the sediment ~ 30 cm apart, and the sediment was allowed to re-equilibrate for at least 1 h before sampling. A peristaltic pump sampled water from each drivepoint simultaneously at approximately 3 mL min^{-1} , and pumped it through neoprene tubing with $0.45\text{ }\mu\text{m}$ Aquaprep groundwater sampling filters (Pall Co., Port Washington, NY) and into six Ar-purged 100 mL septa vials, one for each depth.

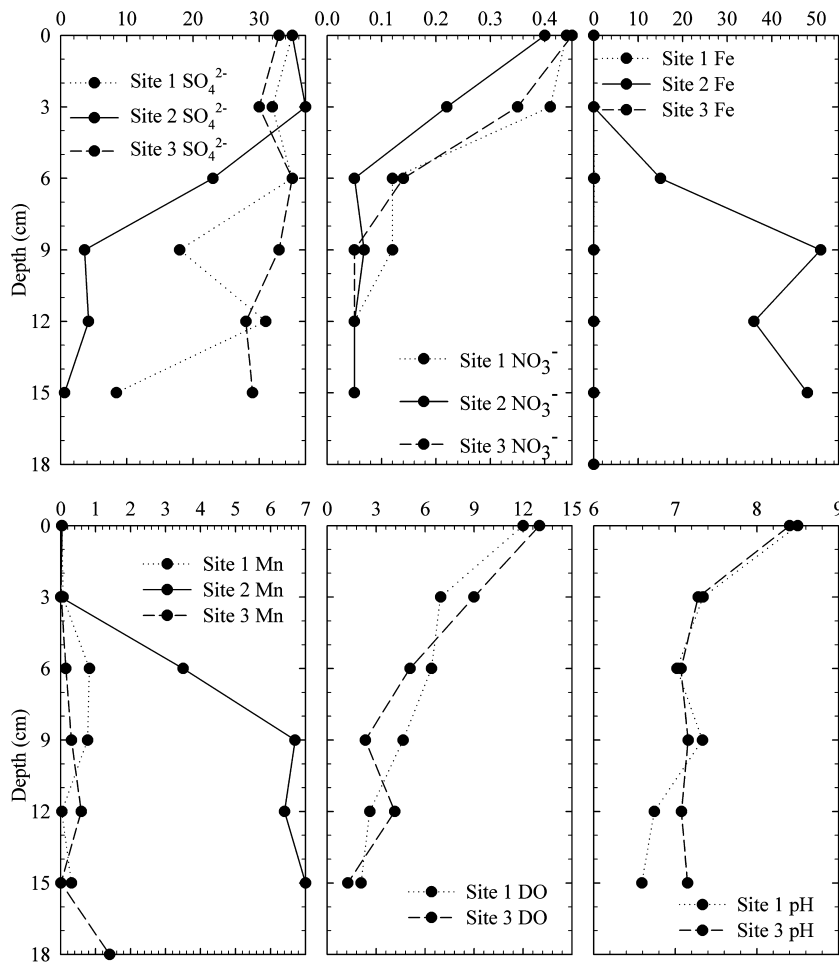


FIGURE 1. June 2008 SW (0 cm) and PW profiles from 3 sampling sites. BDL points are shown as DL/2. DO and pH data are averages of 2 or 3 values with minimal variability. All data are mg L⁻¹ except pH.

Duff et al. (19) showed that using a Minipoint to sample PW in a sand and gravel bed stream at higher pumping rates and at closer depth intervals (2.5 cm) did not disturb the vertical profile of a conservative tracer. The amount of sample collected at each depth ranged from 10 to 80 mL, depending on Minipoint and tube clogging. Pore water pH and DO were measured in line using Teflon flow cells, flushed with 3–5 mL of sample. Each PW sample was aliquoted for measurement of total alkalinity, total and dissolved Se, dissolved metals and anions, and nitrogen speciation.

Sediments were sampled to 18 cm in June 2008 and 24 cm in August 2008 using a slide-hammer corer as described in Oram et al. (3).

Br⁻ Tracer Study. A half-saturated solution of bromide was made by mixing NaBr salt with EMC SW in 250-L Marriott bottles (20). The tracer was discharged into the creek at 43 mL min⁻¹ in June 2008 and 39 mL min⁻¹ in August 2008 for at least 10 h, ~50 m upstream of sampling sites. The injection duration and reach length required for an accurate tracer experiment were calculated following Wagner and Harvey (21). To verify steady-state, Br⁻ was monitored in the field using a combination Br⁻-selective electrode (Cole-Palmer, Vernon Hills, IL). Pore water and SW samples were collected from June 2008 site 1 and August 2008 site 2 to measure background and steady-state Br⁻ concentrations.

Sample Analysis. In the field, SW and PW samples collected for dissolved or total metals were acidified to pH 2 with HNO₃, and nitrogen speciation samples were acidified to pH 2 with H₂SO₄. Field duplicates and field blanks were prepared for each subsample. Total alkalinity was measured

in the field following EPA Method 310.1 on June 2008 and August 2008 unfiltered SW samples and on June 2008 PW samples.

Samples of preserved SW and PW were submitted to the University of Idaho Analytical Sciences Laboratory (UIASL) for analysis of dissolved and total (SW only) Se (EPA 200.8), dissolved and total (SW only) metals (EPA 200.7), anions (including Br⁻) (EPA 300.0), and ammonia (June 2008 samples only) (details in Supporting Information). Sediment cores were frozen, cut into 3-cm sections, and submitted to UIASL for total Se analysis (Supporting Information available). Selenium speciation in six sediment samples (two depths of June 2008 site 1, two depths of June 2008 site 2, and two depths of September 2007 site 1, which was within 50 m of June 2008 and August 2008 sampling sites) was measured with μ -SXRF at Stanford Synchrotron Radiation Lightsource (SSRL).

Micro-SXRF mapping and micro-XANES (X-ray absorption near edge spectra) collection were done on beamline 2–3 at SSRL (Supporting Information available). Gray orthorhombic elemental Se was used to calibrate the monochromator. XRF peak intensities for Ca, Cu, Fe, K, Mn, S, Se, Ti, and Zn were collected at each pixel as the sample was rastered through the beam. Selenium species distribution maps were collected for reduced Se (Se(0) and Se(-II)), Se(IV), and Se(VI) by scanning regions of interest at four different energies (Supporting Information available). Dwell time of the 2 × 2 μm beam was 250 ms per pixel, and step size was 5 μm for 16 larger region maps (0.0769–0.289 mm²), and 1 μm for six higher resolution (HR) maps collected within the larger

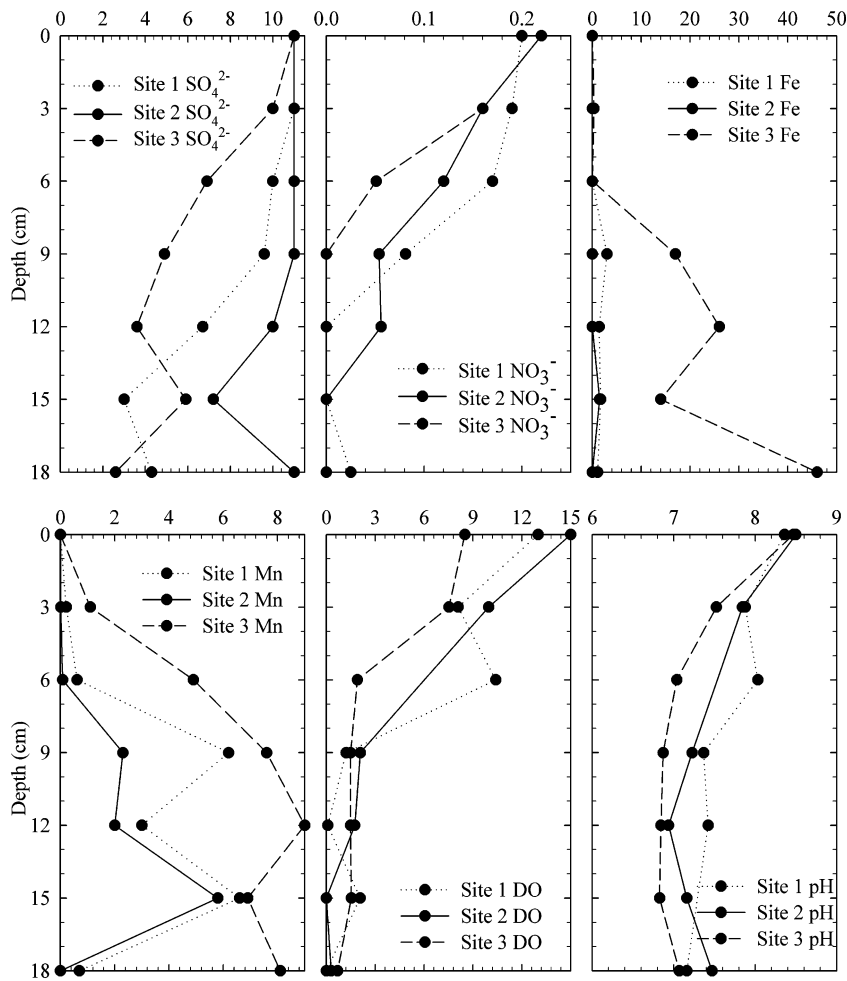


FIGURE 2. August 2008 SW (0 cm) and PW profiles from 3 sampling sites. BDL points are shown as DL/2. DO and pH are averages of triplicates. All data are mg L^{-1} except pH.

regions. Micro-SXRF maps were deconvoluted to reduce signal overlaps using methods described in Sutton et al. (11), as implemented in Oram et al. (3) (Supporting Information available). The percent of each Se species for each μ -SXRF map was calculated using the average pixel intensity of each species. Tricolor maps showing the spatial distribution of three species or elements were produced in SMAK version 0.47 (22). Pixel brightness is displayed in RGB, with the brightest spots corresponding to the highest fluorescence. Quick XANES scans were collected from 44 Se hotspots within the mapped regions and compared to XANES from standards (sodium selenate, sodium selenite, and gray orthorhombic elemental Se) to determine oxidation state.

Results

Surface Water and Pore Water. Dissolved O_2 in SW (reported as 0 cm in Figures 1 and 2) range was 8.6–14.9 mg L^{-1} , and pH range was 8.4–8.5. Surface water alkalinity was 188 ± 5.56 (sd) mg L^{-1} CaCO_3 ($n = 5$) and 184 ± 1.22 mg L^{-1} CaCO_3 ($n = 6$) for June 2008 and August 2008, respectively. Surface water SO_4^{2-} (detection limit (DL) = 0.2 mg L^{-1}) range was 33–35 mg L^{-1} for June 2008, and SO_4^{2-} was 11 mg L^{-1} for August 2008 at all three sites. Surface water NO_3^- (DL = 0.05 mg L^{-1}) range was 0.42–0.45 mg L^{-1} for June 2008 and 0.19–0.22 mg L^{-1} for August 2008. Ammonia was below detection limit (BDL, 0.1 mg L^{-1}) in all June 2008 SW and PW samples. Iron and Mn (DL = 0.02 and 0.005 mg L^{-1} , respectively) were BDL in all SW samples.

Pore water pH, O_2 , SO_4^{2-} , and NO_3^- decreased with depth (Figures 1 and 2). Pore water Mn and Fe increased with depth.

Increase in dissolved Fe and Mn and decrease in O_2 , SO_4^{2-} , and NO_3^- suggest that PW redox conditions transition from oxic to suboxic at ~6 cm. A decrease in sediment pH is commonly attributed to microbial respiration and decaying organic matter. June 2008 PW alkalinity increased between the 3 and 15 cm samples, 197 to 262, 218 to 368, and 183 to 236 mg L^{-1} CaCO_3 for sites 1, 2, 3, respectively. Increase in alkalinity is consistent with increase in heterotrophic respiration in sediments. Low PW nitrate is also consistent with anaerobic respiration enhancing denitrification (17).

Within 1 h after tracer injection, SW Br^- along the 50-m stretch above the sampling sites was constant, and the injections resulted in a ~60 mV decrease from preinjection Br^- readings (Supporting Information available). Stream discharge was $0.0653 \pm 0.00170 \text{ m}^3 \text{ s}^{-1}$ ($n = 5$) in June 2008 and $0.0447 \pm 0.00396 \text{ m}^3 \text{ s}^{-1}$ ($n = 3$) in August 2008. Background Br^- was <0.1 mg L^{-1} (DL) in all SW and ranged from <0.1 to 0.55 mg L^{-1} in all PW (Figures 3 and 4). During steady-state injection, SW Br^- was $3.5 \pm 0.0 \text{ mg L}^{-1}$ ($n = 2$) for June 2008 and $3.4 \pm 0.07 \text{ mg L}^{-1}$ ($n = 2$) for August 2008, and PW Br^- ranged from 3.2 to <0.1 mg L^{-1} for June 2008 and 2.9 to <0.1 mg L^{-1} for August 2008, and decreased with depth during both field events (Figures 3 and 4). Because Br^- is a nonreactive solute tracer (8, 23), the Br^- concentrations represent a nonreactive chemical profile. The portion of a streambed having at least 10% SW contribution is considered the hyporheic zone with significant SW and groundwater (GW) mixing (24). Bromide falls below 10% SW Br^- between 9–12 and 12–15 cm for June 2008 and August 2008,

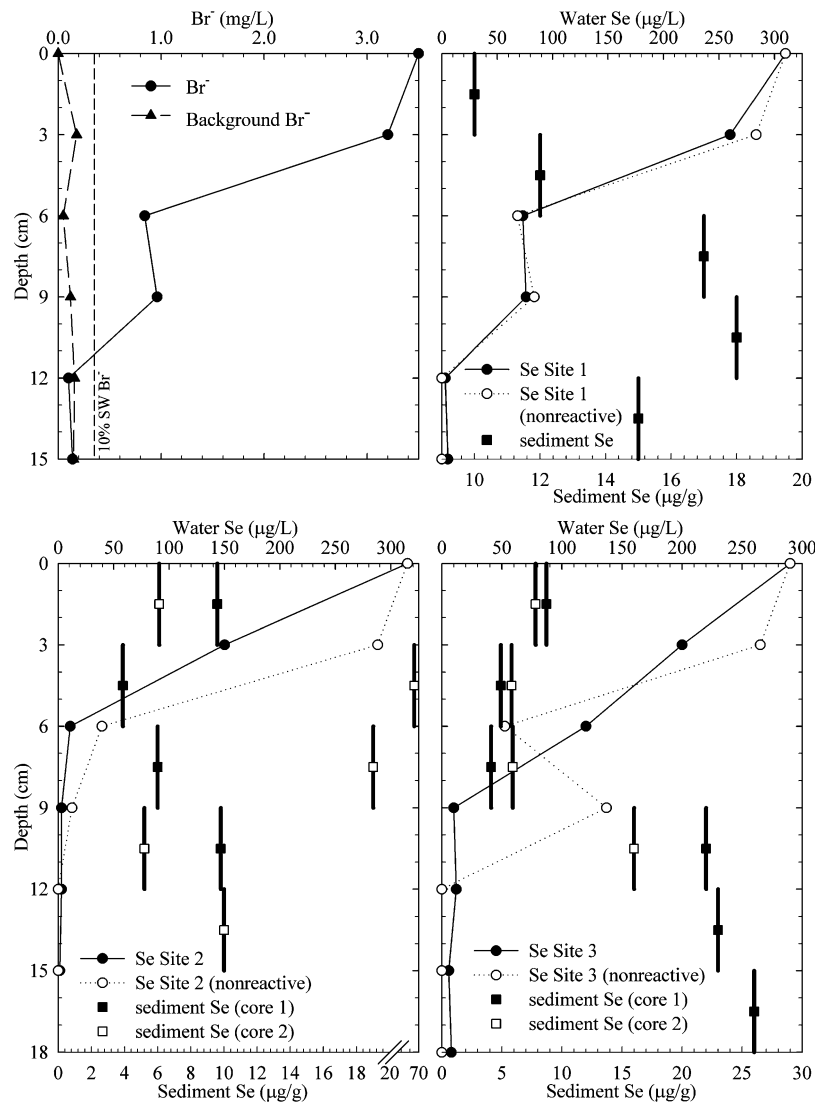


FIGURE 3. June Br^- profiles and SW (depth 0), PW, and sediment Se profiles at three sampling sites. Points BDL are shown as DL/2.

respectively (Figures 3 and 4). Thus, the predicted hyporheic zone extends to 12 ± 3 cm.

Heat can also be used as a tracer to determine the extent of GW-SW interaction (23). Surface water temperatures varied diurnally and seasonally from 4.4 to 6.9 °C in June 2008 and 6.1–7.0 °C in August 2008 (Figures S1 and S2). In 14 thermal profiles collected, temperatures changed by 1–1.5 °C from the sediment surface down to 15–20 cm. Below 15–20 cm, temperatures were relatively constant, suggesting the presence of groundwater that is buffered from SW temperature fluctuations. The predicted hyporheic zone depth estimated by temperature gradients at all sites is consistent with the maximum hyporheic zone predicted using Br^- .

Surface water Se concentrations in June 2008 ranged from 290 to 315 µg Se L⁻¹, and PW Se ranged from 1.5 to 260 µg L⁻¹ (Figure 3). August 2008 SW Se range was 58–67 µg L⁻¹, and PW Se range was 0–56 µg L⁻¹ (Figure 4). Dissolved particulate Se in the SW was negligible. Pore water Se decreased with depth at all three sites for both dates, and concentration gradients are similar to the nonreactive tracer (Figures 3 and 4). The O_2 , SO_4^{2-} , and NO_3^- profiles (Figures 1 and 2) also follow the Se and Br^- profiles (Figures 3 and 4).

To estimate whether Se uptake or release occurred at each depth, modeling was done to calculate nonreactive Se concentrations. The model used Br^- concentrations and a steady-state transport model developed by Harvey and Fuller

(8), which was applied to predict hyporheic zone metal reactions in Fuller and Harvey (15):

$$\hat{C}_{\text{h}}^{i+1} = C_{\text{h}}^i + \beta^{i+1/2}(C_{\text{L}} - C_{\text{h}}^i) - \lambda_{\text{h}}^{i+1/2}\tau_{\text{h}}^{i+1/2}(C_{\text{h}}^i + C_{\text{h}}^{i+1})/2$$

Where C_{h}^i is the concentration of Se in the hyporheic zone, C_{L} is the GW concentration, τ_{h} is the tracer travel time, β is the fraction of GW in a depth increment, and λ_{h} is the reaction rate constant. Because we calculated nonreactive profiles, $\lambda_{\text{h}} = 0$. The circumflex ($\hat{\cdot}$) indicates a calculated concentration, the superscript i represents a specific sampling depth, $i + 1$ the next deeper depth, and $i + 1/2$ the average value for the interval between sampling depths. Comparing predicted nonreactive Se and actual Se concentrations at each depth allows the determination of Se release or uptake. Estimated error in predicted Se and Br^- profiles are <10%, and differences greater than 10% indicate release or uptake. When PW Se is greater than predicted nonreactive Se, Se release from the sediment is implied. When PW Se is less than predicted nonreactive Se, Se sequestration is implied. The fraction of GW at each depth, $\beta^{i+1/2}$, was calculated using the Br^- data:

$$\beta^{i+1/2} = (\text{Br}_{\text{h}}^{i+1} - \text{Br}_{\text{h}}^i)/(\text{Br}_{\text{L}} - \text{Br}_{\text{h}}^i)$$

The lowest Minipoint samplers (15 or 18 cm) were below the predicted hyporheic zone at all sites, and thus, the deepest

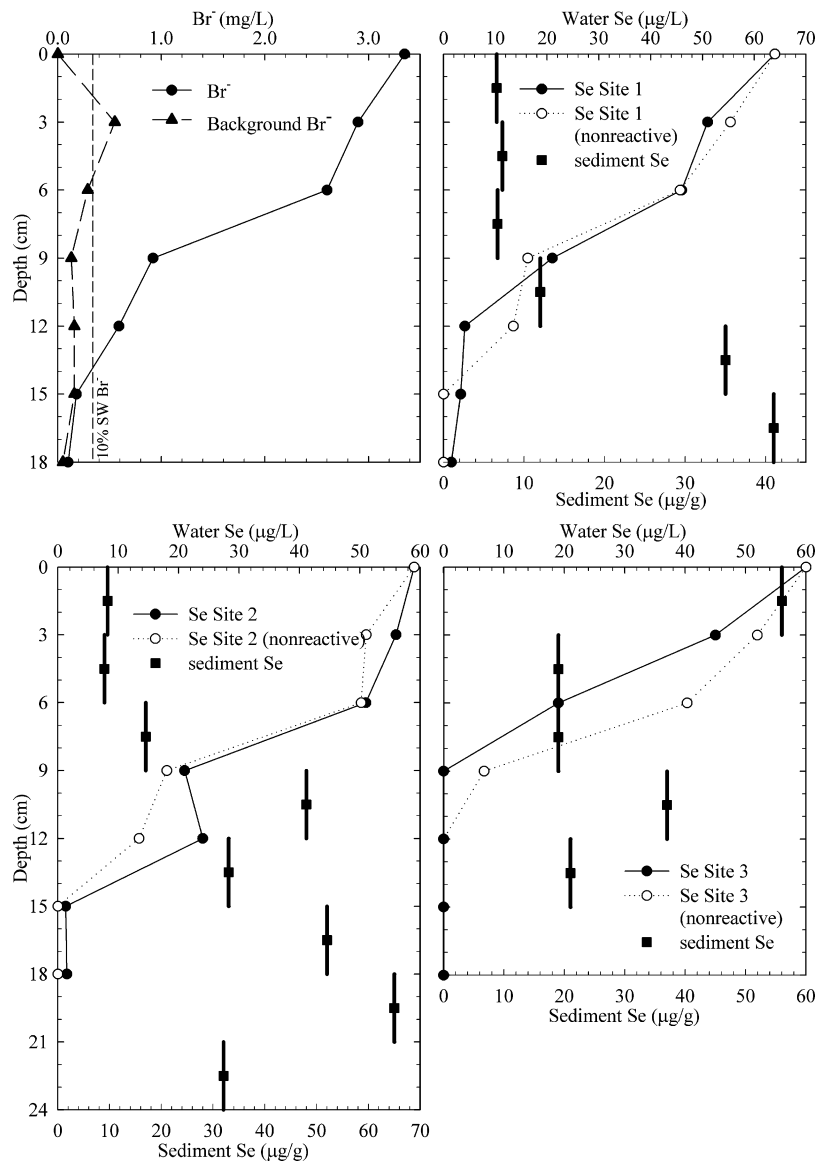


FIGURE 4. August Br^- profiles and SW (depth 0), PW, and sediment Se profiles at three sampling sites. Points BDL are shown as DL/2.

PW Se concentrations are reliable estimates of GW Se flowing into the hyporheic zone. Selenium concentrations in the deepest PW samples were much lower than SW concentrations (Figures 3 and 4). Thus, C_L was estimated to be zero, and the nonreactive profiles represent minimum concentrations. If GW Se concentrations were greater than zero, calculated nonreactive Se (\hat{C}_{H}^{i+1}) would increase. Using zero for C_L allows modeling of either minimum uptake or maximum release.

In seven of 13 samples below the hyporheic zone, PW Se ranged from 3.0 to 12 $\mu\text{g L}^{-1}$. The predicted nonreactive Se is zero below the hyporheic zone, and the difference between observed and predicted Se suggests Se release and/or uptake, or potential GW Se influx. However, Se concentrations were much less than hyporheic zone and SW concentrations (Figures 3 and 4), indicating a minimal contribution. In 21 sample points within the hyporheic zone, nine showed Se uptake, four showed Se release, and eight were less than 10% different (Figures 3 and 4). Selenium uptake is therefore the predominant process affecting PW Se concentrations within the hyporheic zone. To assess the sensitivity of the model to GW Se input, nonreactive Se profiles were calculated using hypothetical GW Se equal to 1/3 SW concentrations, 100 mg L^{-1} for June 2008 and 20 mg L^{-1} for August 2008. In this

scenario, the model predicts extensive Se uptake at 27 points and Se release at only one point.

Sediment. Sediment Se for June 2008 samples ranged from 3.9 to 69 $\mu\text{g g}^{-1}$ (Figure 3). Sediment Se for August 2008 samples ranged from 6.6 to 65 $\mu\text{g g}^{-1}$ (Figure 4). Most sediment cores had increasing Se concentrations with depth (Figures 3 and 4). In six of eight total cores, sediment Se was inversely related to PW Se, with R ranging from -0.27 to -0.79 ($n = 6$, $p < 0.05$).

Example oxidation-state maps are shown in Figure 5. The HR maps in Figure 5 show hotspots of all three species in June 1A1, a Se(-II,0) hotspot in June 1A4, a Se(IV) hotspot in June 2A3, and Se(IV) and Se(-II,0) hotspots in Sept 1A3. All maps had high Fe signals, and usually significant signals attributed to Ca, K, Mn, and Zn fluorescence. An example multichannel analyzer (MCA) XRF spectrum is shown at the bottom of column 2, Figure 5.

The mean percent of each Se species represents the average oxidation state of the mapped region and can be used to compare Se speciation between the maps (Figure 6 and Table S4). Of 16 mapped regions (not including HR maps), 13 contained predominantly Se(-II,0), ranging 42–96%, and 3 contained predominantly Se(IV) at 54%, 57%, and 65% (Figure 6). Se(VI) was observed in few pixels, averaging 1.0–30%,

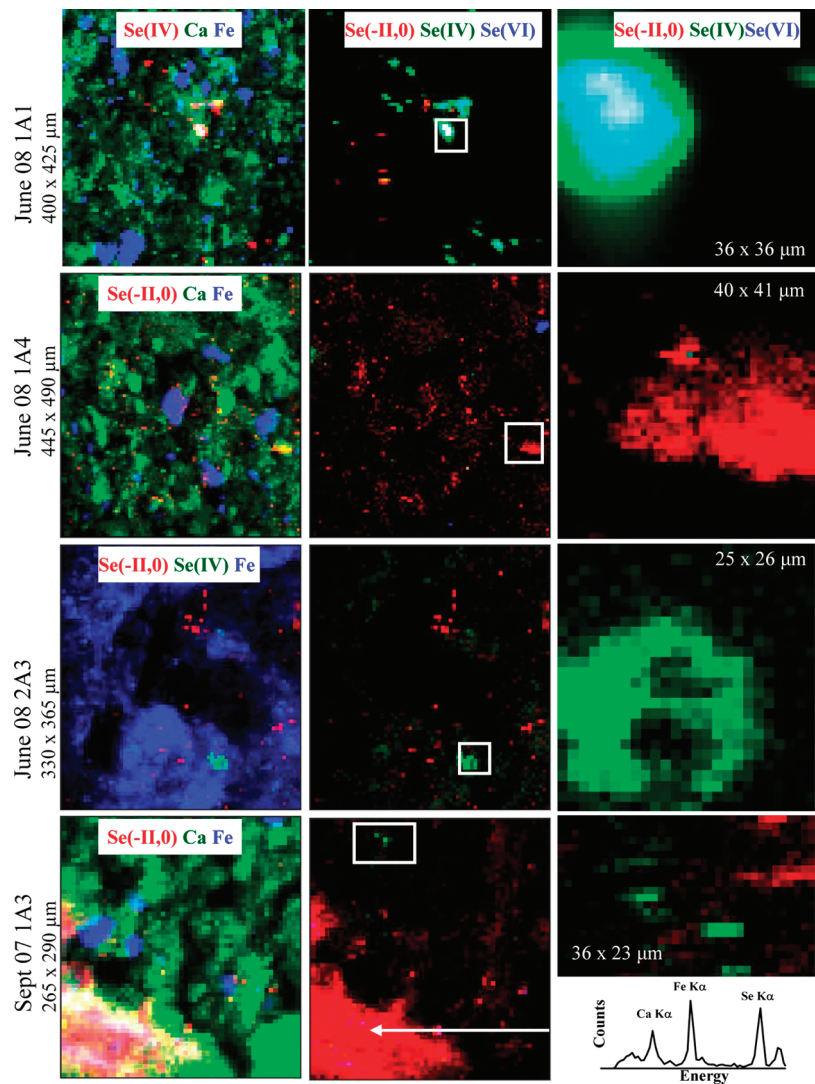


FIGURE 5. Tricolor μ -SXRF maps of distribution and intensity of Se, Fe, and Ca in column one and Se(-II,0), Se(IV), and Se(VI) in columns two and three. Column three shows the HR map of the outlined hotspot in column two. Each row is a different subsample (see Table S4). The inset line plot from Sept 2007 1A3 is an XRF spectrum of the high Se pixel indicated by the white arrow.

and maps with the highest Se(VI) composition had relatively low intensity (Table S4), suggesting a low Se(VI) concentration compared to maps with higher counts.

Although all three species of Se were observed, Se(-II,0) was prominent in samples from all depths (Figure 6). Se(IV) was the predominant species in four maps, all from 0–3 cm samples (three maps from two June 2008 cores and one HR map from a Sept 2007 core (Table S4)). Se(IV) in the deeper samples, 13–15 and 22–24 cm, was less than 31%. Only two samples had significant hotspots (larger than one or two pixels) of Se(VI) (June 1A1 and June 1A4), which was a minor species in the samples.

Various Se hotspots within the maps were examined for correlations between Se and other elements in SMAK. Correlations were observed between Se and Fe, Mn, Zn Ti, Ca, K, S, and Cu. Tricolor maps in Figure 5, column three show the codistribution of Se species with Fe and Ca. Example correlation matrices are shown in Table S2. In general, Se(-II,0) and Se(IV) hotspots were highly correlated with other elements (i.e., $R > 0.8$), but were not co-located. The association between Se(-II,0) and other elements suggests that either inorganic or organic selenides are more prevalent than Se(0).

Micro-XANES scans from points of interest (POIs) (Table S3 and Figure S3) are useful to confirm results of oxidation state mapping and data processing. The XANES from 40 of

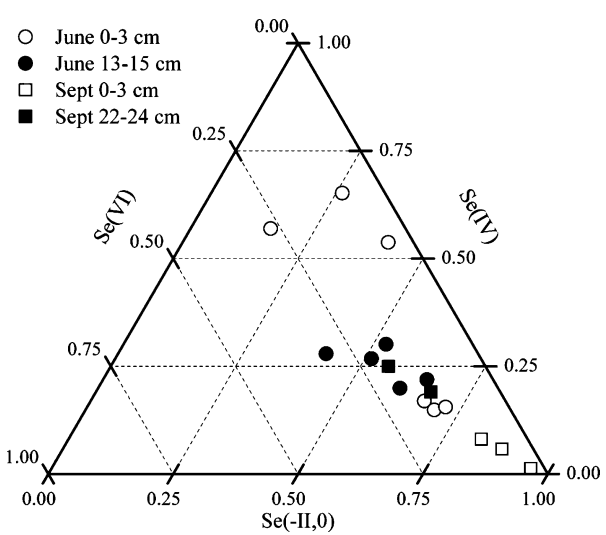


FIGURE 6. Ternary diagram of the average Se speciation from 16 oxidation state maps from six sediment samples. Each point represents the average fraction of each Se species from the oxidation state maps. More than 3000 pixels were averaged for each map point shown. Data are reported in Table S4.

the 44 POIs were in agreement with map results; that is, if a map hotspot was interpreted to be Se(-II,0), the XANES POI also showed Se(-II,0) as the predominant oxidation state (Supporting Information available). All XANES from 13–15 or 22–24 cm samples show either all Se(-II,0) or a mixture of Se(-II,0) and Se(IV). In agreement with μ -SXRF mapping, XANES spectra with Se(IV) and Se(VI) oxidation states (10 of 44 spectra), were all from 0–3 cm samples (Supporting Information available).

Discussion

The depth of hyporheic exchange in EMC sample sites is 12 ± 3 cm, confirmed by both Br[−] and thermal profiles. On the basis of SW velocity and estimated exchange rates (Supporting Information available), PW and SW are predicted to exchange numerous times within the EMC drainage basin, creating ample hyporheic exchange to facilitate significant changes in total Se loads. Surface water provides a continual input of Se into the hyporheic zone that may be sequestered via adsorption, reduction, absorption, precipitation, or biological uptake. Selenium release can occur if conditions are favorable for desorption, oxidation, or dissolution (1). On the basis of comparison of the actual and modeled nonreactive Se profiles (Figures 3 and 4), hyporheic zone sequestration is occurring, although some spatial variability was observed.

Redox potentials for Se reduction are between those for Fe and SO₄^{2−} (1, 7). Pearson correlation coefficients for dissolved Fe and Se in EMC PW are −0.68 for August 2008 site 1, −0.70 for August 2008 site 3, and −0.78 for June 2008 site 2. Thus, reduction of Fe and SO₄^{2−} in the lower sediment profile demonstrates that conditions are favorable for Se reduction, which may occur abiotically or by sulfate reducing bacteria (25). Reduced Se exists as the oxyanion selenite, which is strongly adsorbed to mineral surfaces; elemental Se or inorganic selenides, which have low solubilities; or organic selenides, which may occur as bioavailable biomolecules that are typically unstable and quickly mineralized, absorbed, or volatilized or as complex stable substances such as kerogen (1, 26).

Dissolved Se observed in lotic systems is mainly reported to be selenate (14, 27, 28). Pore water Se is reduced from selenate to selenite, elemental Se, or selenide as sediments become more reducing (1, 7). The high solubility of selenate corresponds to greater Se concentrations in near-surface PW, where DO and SW influx are high, and lower solid-phase Se in the near-surface sediment (average 0–6 cm Se concentration is $8.6 \pm 3.7 \mu\text{g g}^{-1}$, $n = 14$ (two outliers removed, $p < 0.5$)). Increased Se(IV) in the surface sediments and the extensive distribution of Se(-II,0) in all sediments, as indicated by μ -SXRF and μ -XANES (Figure 6 and Figure S3), confirms that active biogeochemical reactions are reducing Se throughout the profile. Therefore, redox and depth-dependent Se sequestration reactions promote increased solid-phase Se at depth, explaining the inverse relationship between sediment Se and PW Se. Although the data suggest reduction and sequestration are more prominent with depth in the hyporheic zone, historical deposition of Se-enriched sediments from a century of mining also may have contributed to sediment profiles (Supporting Information available).

This research shows that the Se concentration gradient in the EMC hyporheic zone is affected by both direct SW–PW exchange and biogeochemical reactions. Field and microscale geochemistry suggest that aqueous selenate is reduced in the sediments to selenite at shallow depths and to either metal or organic selenides at deeper depths. These reactions are important original observations of Se biogeochemical cycling and flux in the hyporheic zone of

lotic ecosystems, wherein flow dynamics influence Se biogeochemistry (14).

Given that lotic stream systems are highly heterogeneous at various environmental scales, characterization of other sites within EMC and other streams in the watershed is needed. Additionally, further research should measure specific reaction mechanisms and rates, the relative contributions of abiotic and biotic mechanisms, and the impact of environmental fluxes on biogeochemical reactions.

Acknowledgments

Funding was provided by USGS, IDEQ, and the Jeff Braatne Ph.D. Memorial Grant. SSRL is a national user facility operated by Stanford University on behalf of the US Department of Energy, Office of Basic Energy Sciences. Assistance on this project was graciously provided by Leslie Baker at University of Idaho, Christopher Fuller at USGS, and Sam Webb at SSRL. We thank Bear Lake Grazing for allowing access to the research site. Gregory Möller has in the past consulted for organizations representing and contracting with industry, the U.S. Environmental Protection Agency, and the U.S. Department of Health and Human Services - Agency for Toxic Substances and Disease Registry on issues relating to selenium release, exposure, and risk assessment.

Supporting Information Available

Additional site description, sampling, analysis, tracer, X-ray spectroscopy, seasonal, and hyporheic exchange details are included. Additional figures include temperature profiles and XANES. Additional tables include signal-correction matrix, correlation matrices, and tabulated XANES oxidation states. This material is available free of charge via the Internet at <http://pubs.acs.org>.

Literature Cited

- (1) Maher, W.; Roach, A.; Doblin, M. A.; Fan, T.; Foster, S.; Garrett, R.; Möller, G.; Oram, L.; Wallschläger, D. Environmental sources, speciation and partitioning of selenium. In *Ecological Assessment of Selenium in the Aquatic Environment*; Chapman, P., Adams, W., Brooks, M., Delos, C., Luoma, S., Maher, W., Ohlendorf, H., Presser, T., Shaw, D., Eds.; SETAC Press: Pensacola, FL, 2010.
- (2) Stilling, L. L.; Amacher, M. C. Kinetics of selenium release in mine waste from the Meade Peak Phosphatic Shale, Phosphoria Formation, Wooley Valley, Idaho, USA. *Chem. Geol.* **2010**, *269*, 113–123.
- (3) Oram, L.; Strawn, D. G.; Marcus, M. A.; Möller, G. Macro- and microscale investigation of selenium speciation in Blackfoot river, Idaho, sediments. *Environ. Sci. Technol.* **2008**, *42*, 6830–6836.
- (4) Hamilton, S. J.; Buhl, K. J. Selenium in water, sediment, plants, invertebrates, and fish in the Blackfoot River drainage. *Water, Air, Soil Pollut.* **2004**, *159*, 3–34.
- (5) Kazeyilmaz-Ahlan, C. M.; Medina, M. A. Stream solute transport incorporating hyporheic zone processes. *J. Hydrol.* **2006**, *329*, 26–38.
- (6) Feris, K.; Ramsey, P.; Frazar, C.; Rilling, M.; Gannon, J.; Holben, W. Structure and seasonal dynamics of hyporheic zone microbial communities in free-stone rivers of the western United States. *Microbial Ecol.* **2003**, *46*, 200–215.
- (7) Masschelein, P. H.; Patrick, W. H. Biogeochemical processes affecting selenium cycling in wetlands. *Environ. Toxicol. Chem.* **1993**, *12*, 2235–2243.
- (8) Harvey, J. W.; Fuller, C. C. Effect of enhanced manganese oxidation in the hyporheic zone on basin-scale geochemical mass balance. *Water Resour. Res.* **1998**, *34*, 623–636.
- (9) Mukherjee, A.; Fryar, A. E.; Lasage, D. M. Using tracer tests to assess natural attenuation of contaminants along a channelized coastal plain stream. *Environ. Eng. Geosci.* **2005**, *XI*, 371–382.
- (10) Pickering, I. J.; Prince, R. C.; Salt, D. E.; George, G. N. Quantitative, chemically specific imaging of selenium transformation in plants. *Proc. Natl. Acad. Sci. U.S.A.* **2000**, *97*, 10717–10722.
- (11) Sutton, S. R.; Bajt, S.; Delaney, J.; Schulze, D.; Tokunaga, T. K. Synchrotron x-ray fluorescence microprobe: quantification and mapping of mixed valence state samples using micro-XANES. *Rev. Sci. Instrum.* **1995**, *66*, 1464–1467.

- (12) Belzile, N.; Chen, Y.-W.; Rongrong, X. Early diagenetic behavior of selenium in freshwater sediments. *Appl. Geochem.* **2000**, *15*, 1439–1454.
- (13) Tokunaga, T. K.; Sutton, S. R.; Bajt, S.; Nuessle, P.; Shea-McCarthy, G. Selenium diffusion and reduction at the water-sediment boundary: Micro-XANES spectroscopy of reactive transport. *Environ. Sci. Technol.* **1998**, *32*, 1092–1098.
- (14) Simmons, D.; Wallschlager, D. A critical review of the biogeochemistry and ecotoxicology of selenium in lotic and lentic environments. *Environ. Toxicol. Chem.* **2005**, *24*, 1331–1343.
- (15) Fuller, C. C.; Harvey, C. F. Reactive uptake of trace metals in the hyporheic zone of a mining-contaminated stream, Pinal Creek, Arizona. *Environ. Sci. Technol.* **2000**, *34*, 1150–1155.
- (16) Miller, M. P.; McKnight, D. M.; Cory, R. M.; Williams, M. W.; Runkel, R. L. Hyporheic exchange and fulvic acid redox reactions in an alpine stream/wetland ecosystem, Colorado Front Range. *Environ. Sci. Technol.* **2006**, *40*, 5943–5949.
- (17) O'Connor, B. L.; Hondzo, M. Enhancement and inhibition of denitrification by fluid-flow and dissolved oxygen flux to stream sediments. *Environ. Sci. Technol.* **2008**, *42*, 119–125.
- (18) Nu-West Industries Inc.; HWS Consulting Group Inc. *North Maybe Mine Draft Final Site Investigation Report*, **2006**.
- (19) Duff, J. H.; Murphy, F.; Fuller, C. C.; Triska, F. J. A mini drivepoint sampler for measuring pore water solute concentrations in the hyporheic zone of sand-bottom streams. *Limnol. Oceanogr.* **1998**, *43*, 1378–1383.
- (20) McCarthy, E. L. Mariotte's Bottle. *Science* **1934**, *80*, 100.
- (21) Wagner, B.; Harvey, J. W. Experimental design for estimating parameters of rate-limited mass transfer: Analysis of stream tracer studies. *Water Resour. Res.* **1997**, *33*, 1731–1741.
- (22) Webb, S. Sam's Microprobe Analysis Kit (SMAK); Stanford Synchrotron Radiation Laboratory, 2009.
- (23) Constantz, J.; Cox, M. H.; Su, G. W. Comparison of heat and bromide as ground water tracers near streams. *Ground Water* **2003**, *41*, 647–656.
- (24) Triska, F.; Duff, J. H.; Avanzino, R. The role of water exchange between a stream channel and its hyporheic zone in nitrogen cycling at the terrestrial-aquatic interface. *Hydrobiologia* **1993**, *251*, 167–184.
- (25) Hockin, S.; Gadd, G. M. Removal of selenate from sulfate-containing media by sulfate-reducing bacterial biofilms. *Environ. Microbiol.* **2006**, *8*, 816–826.
- (26) Wen, H.; Carignan, J.; Qiu, Y.; Liu, S. Selenium speciation in kerogen from two Chinese selenium deposits: environmental implications. *Environ. Sci. Technol.* **2006**, *40*, 1126–1132.
- (27) Amouroux, D.; Donard, O. Evasion of selenium to the atmosphere via biomethylation processes in the Gironde estuary, France. *Mar. Chem.* **1997**, *58*, 173–188.
- (28) Nishri, A.; Brenner, I.; Hall, G.; Taylor, H. Temporal variations in dissolved selenium in Lake Kinneret (Israel). *Aquat. Sci.* **1999**, *61*, 215–233.

ES100149U